Geochemistry Geophysics Geosystems G3

Article
Volume 14, Number 12
27 December 2013
doi: 10.1002/2013GC004973
ISSN: 1525-2027

Published by AGU and the Geochemical Society

Critical single domain grain sizes in chains of interacting greigite particles: Implications for magnetosome crystals

Adrian R. Muxworthy
Department of Earth Science and Engineering, Imperial College London, South Kensington Campus, London SW7 2AZ, UK (adrian.muxworthy@imperial.ac.uk)

Wyn Williams
Grant Institute of Earth Science, University of Edinburgh, Edinburgh, UK

Andrew P. Roberts
School of Ocean and Earth Science, National Oceanography Centre, University of Southampton, Southampton, UK

Research School of Earth Sciences, Australian National University, Canberra, ACT, Australia

Michael Winklhofer
Department of Earth and Environmental Sciences, Ludwig-Maximilian-Universität München, Munich, Germany

Liao Chang
School of Ocean and Earth Science, National Oceanography Centre, University of Southampton, Southampton, UK

Research School of Earth Sciences, Australian National University, Canberra, ACT, Australia

Mihály Pósfai
Department of Earth and Environmental Sciences, University of Pannonia, Veszprém, Hungary

[1] Magnetotactic bacteria contain chains of magnetically interacting crystals (magnetosomes), which aid navigation (magnetotaxis). To improve the efficiency of magnetotaxis, magnetosome crystals (which can consist of magnetite or greigite) should be magnetically stable single domain (SD) particles. Larger particles subdivide into nonuniform multidomain (MD) magnetic structures that produce weaker magnetic signals, while small SD particles become magnetically unstable due to thermal fluctuations and exhibit superparamagnetic (SP) behavior. In this study, we determined the stable SD range as a function of grain elongation and interparticle separation for chains of identical greigite grains using fundamental parameters recently determined for greigite. Interactions significantly increase the stable SD range. For example, for cube-shaped greigite grains the upper stable SD threshold size is increased from 107 nm for isolated grains to 204 nm for touching grains arranged in chains. The larger critical SD grain size for greigite means that, compared to magnetite magnetosomes, greigite magnetosomes can produce larger magnetic signals without the need for intergrain interactions.

Components: 8,212 words, 7 figures.

Keywords: greigite; magnetosome; single domain.

Index Terms: 1540 Rock and mineral magnetism: Geomagnetism and Paleomagnetism; 1505 Biogenic magnetic minerals: Geomagnetism and Paleomagnetism; 1519 Magnetic mineralogy and petrology: Geomagnetism and Paleomagnetism; 5109 Magnetic and electrical properties: Physical Properties of Rocks; 0925 Magnetic and electrical methods: Exploration Geophysics.

Received 5 August 2013; **Revised** 30 October 2013; **Accepted** 30 October 2013; **Published** 27 December 2013.

Muxworthy, A. R., W. Williams, A. P. Roberts, M. Winklhofer, L. Chang, and M. Pósfai (2013), *Geochem. Geophys. Geosyst.*, *14*, 5430–5441, doi:10.1002/2013GC004973.

1. Introduction

[2] Magnetotactic bacteria produce chains of magnetic crystals (magnetosomes) that usually consist of magnetite (Fe_3O_4) or greigite (Fe_3S_4) (Figure 1). These magnetosome chains are found in both unicellular bacteria and in larger multicellular magnetotactic prokaryotes (MMP) [*Silveira et al*., 2007; *Faivre and Schüler*, 2008; *Perantoni et al*., 2009]. The primary purpose of magnetosomes is thought to be navigation (magnetotaxis), therefore natural selection should ensure that magnetosomes provide a strong magnetic signal to maximize their efficiency [*Kopp and Kirschvink*, 2008]. The magnetic state that best exhibits this property is the stable single domain (SD) state. The magnetic domain state of a crystal is strongly dependent on both size and shape [*Butler and Banerjee*, 1975]. When SD particles are smaller than a critical threshold size, they are no longer magnetically stable because thermal energy can easily overcome the energy barrier that otherwise prevents domain switching. Such particles then have superparamagnetic (SP) behavior. Larger grains above the SD threshold size form complex nonuniform or multidomain (MD) structures, which leads to inefficient magnetotaxis [*Frankel et al*., 1998] because the magnetic remanence per unit volume is far less than that in SD grains. Determining the critical stable SD size range as a function of morphology is important for determining magnetosome function and possible magnetotaxis efficiency. Critical sizes for stable SD behavior are also of interest to Earth and materials scientists because stable SD grains have the most ideal recording fidelity, and because the easily identifiable magnetic characteristics of stable SD grains are useful indicators of grain size.

[3] It is common to assess the domain state of magnetosome crystals by plotting their length versus grain elongation axial ratio (AR; short-axis/long-axis or width/length) on domain-state phase diagrams [*Thomas-Keprta et al*., 2000], which were initially determined analytically by *Evans and McElhinny* [1969] and *Butler and Banerjee* [1975]. *Butler and Banerjee* [1975] calculated the SP to stable SD critical size and the SD to MD critical size as functions of AR for individual particles of magnetite and titanomagnetite. Subsequently, both the SP to stable SD transition size [*Winklhofer et al*., 1997; *Muxworthy et al*., 2003a] and the SD to MD transition size [*Fabian et al*., 1996; *Newell and Merrill*, 1999; *Witt et al*., 2005; *Muxworthy and Williams*, 2006] have been reexamined and revised for individual magnetite particles through application of the numerical micromagnetic equations of *Brown* [1963].

[4] *Muxworthy and Williams* [2006] demonstrated that it is deceptive to compare magnetosome sizes with critical grain size boundaries derived for individual crystals because magnetosomes nearly always occur in magnetostatically interacting chains [*Dunin-Borkowski et al*., 1998; *Faivre and Schüler*, 2008]. *Muxworthy and Williams* [2006, 2009] performed calculations to include chains of

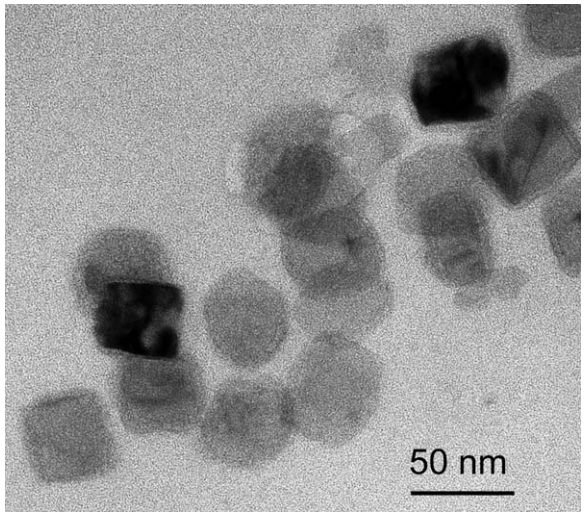

Figure 1. TEM image of part of a slightly disordered, multiple chain of greigite magnetosomes from an uncultivated, rod-shaped marine magnetotactic bacterium.

magnetically interacting rectangular cuboids of magnetite, and demonstrated that for cube-shaped grains, interactions within chains increases the stable SD to MD threshold size for magnetite from ~70 nm to a maximum of ~200 nm. *Muxworthy and Williams* [2006, 2009] showed that magnetostatic interaction fields are sufficient to cause the largest observed magnetite magnetosome crystals found in living bacteria [length = 250 nm (AR = 0.84); *Lins et al*., 2005] to be in a stable SD state; without magnetostatic interactions they would be in a MD state and would have a far lower magnetotaxis efficiency. Interactions also decrease the SP/SD size for cube-shaped magnetite grains from ~26 nm to a minimum of ~12 nm for a thermal relaxation time of 60 s. That interactions decrease the SP/SD threshold size supports earlier observational data for magnetosomes [*Dunin-Borkowski et al*., 1998; *McCartney et al*., 2001]. The fossil record contains a limited number of exceptions [*Schumann et al*., 2008; *Chang et al*., 2012]; these studies reported several morphologies, including a spearhead-like magnetite magnetofossil that occurs with lengths up to 4000 nm (AR ~0.4). The function of this spearhead-like magnetofossil is unlikely to be magnetotaxis [*Chang et al*., 2012], and there are indeed contemporary examples of metazoans that use magnetic minerals for their hardness, rather than for their magnetic properties, e.g., chiton (marine molluscs that cling to rocks) have magnetite-coated "teeth" [*Lowenstam*, 1962], and scaly foot gastropods found at deep ocean vents have greigite-bearing sclerites on their foot [*Warén et al*., 2003; *Suzuki et al*., 2006].

[5] In order to determine the ideal particle size range for magnetotaxis, it is important to make micromagnetic calculations for all relevant magnetic biominerals. This size range is now well known for magnetite [*Muxworthy and Williams*, 2006, 2009], but the range for greigite has not yet been established. *Diaz-Ricci and Kirschvink* [1992] made analytical estimates similar to those of *Butler and Banerjee* [1975] for individual greigite particles; however, their calculations were based on crude estimations of the fundamental parameters of greigite, which were not well constrained at the time due to the lack of chemically pure samples and instead were deduced from comparison with magnetite [for more detailed discussion, see *Chang et al*., 2008; *Roberts et al*., 2011]. *Diaz-Ricci and Kirschvink* [1992] determined the SD/MD threshold to be ~250 nm for cube-shaped grains. More robust analytical and micromagnetic calculations of the SD state phase diagram for greigite are now possible because all of the required fundamental magnetic parameters have recently been determined on chemically pure samples [*Chang et al*., 2008, 2009; *Roberts et al*., 2011; M. Winklhofer et al., On the magnetocrystalline anisotropy constant of greigite (cubic Fe3S4), submitted to *Journal of Geophysical Research*, 2013].

[6] As is the case for magnetite magnetosomes, greigite magnetosomes often occur as rectangular cuboids [*Bazylinski et al*., 1995] or in cubo-octahedral shapes [*Pósfai et al*., 1998] in interacting chains [*Kasama et al*., 2006a]. Furthermore, inorganic greigite often occurs in strongly interacting clusters of cubo-octahedral grains [e.g., *Rowan and Roberts*, 2006; *Roberts et al*., 2011]. Both of these common scenarios make it important to understand how the SD size range is affected by interactions. In this paper, we present results for chains of greigite magnetosomes. Using the physical parameters measured by *Chang et al*. [2008, 2009] and *Winklhofer et al*. (Winklhofer et al., submitted manuscript, 2013), we have determined the domain-state phase diagram for chains of rectangular greigite cuboids with varying interaction spacings and AR values. We model interacting elongated rectangular cuboids as an approximation to magnetosome crystals. For individual magnetite grains, rectangular cuboids have been shown to yield slightly lower estimates for the SD/MD threshold size than numerical estimates for more magnetosome-like morphologies [*Witt et al*., 2005], yet the differences for magnetite are small compared to the effect of magnetic interactions [*Muxworthy and Williams*, 2006]. The same is likely to be true for greigite.

[7] While greigite magnetosomes are commonly found in double or multiple chains [*Kasama et al*., 2006a, 2006b], direct imaging of their magnetic structures using off-axis electron-holography [*Kasama et al*., 2006a, 2006b] indicates that the magnetic interaction fields along the individual chains are much stronger than between the strands in a chain, i.e., as a first-approximation the inter-chain chain interactions can be ignored allowing us to use the same micromagnetic approaches detailed by *Muxworthy and Williams* [2006, 2009] for chains of magnetite crystals.

[8] Absolute values for magnetite's SD/MD threshold size for individual rectangular cuboids determined by *Witt et al*. [2005] are less than those of *Muxworthy and Williams* [2006]. The

rectangular cuboid threshold predictions of *Muxworthy and Williams* [2006] are closer to the predictions of *Witt et al*. [2005] for magnetosome-like morphologies rather than to their predictions for rectangular cuboids. This difference between the two model predictions for rectangular cuboids is most likely because *Witt et al*. [2005] used a conjugate-gradient rather than the dynamic numerical solver used by *Muxworthy and Williams* [2006]; rapid conjugate-gradient solvers are now generally considered to produce less robust solutions than dynamic solvers [*Suess et al*., 2002].

[9] Subsequent to publication of *Muxworthy and Williams* [2009], who used a micromagnetic approach to calculate the SP/SD threshold size for interacting chains of magnetite, *Newell* [2009] proposed an entirely different algorithm for making such calculations using polynomial homotopy continuation. While *Muxworthy and Williams* [2009] calculated the switching field of the chain to estimate the thermal fluctuation field needed to overcome this field, *Newell* [2009] directly calculated the energy barriers between possible magnetic states in the chain. For a chain of touching cubic crystals of magnetite, he determined an SP/SD transition size of ~10 nm for a measurement time of 10^5 s, compared to ~18 nm in *Muxworthy and Williams* [2009]. The approaches of *Muxworthy and Williams* [2009] and *Newell* [2009] both make assumptions, e.g., the paths calculated by *Newell* [2009] are only guides and are not the actual path followed by the magnetization during thermally assisted transitions. These approximations may be the reason why *Newell* [2009] determined a higher energy barrier than *Muxworthy and Williams* [2009]. For consistency and direct comparison with the results of *Muxworthy and Williams* [2009], we use their approach here to determine the SP/SD threshold size for interacting grains.

2. The Micromagnetic Model

[10] The numerical algorithms used in this paper are identical to those described by *Muxworthy and Williams* [2006, 2009], except that we use the physical parameters for greigite instead of magnetite. In the model, a grain is subdivided into a number of subcubes. Each subcube represents the averaged magnetization direction of many hundreds of atomic magnetic dipole moments. All of the subcubes have magnetic moments of equal magnitude, but the magnetization of the different subcubes can vary in direction. To determine the magnetic structures using this finite difference model, two approaches were considered; a combination of both a conjugate-gradient (CG) algorithm [*Williams and Dunlop*, 1989] and a dynamic algorithm [*Suess et al*., 2002], and the CG algorithm alone. The reason for the combined approach is that the dynamic algorithm gives a more rigorous solution; however, it is computationally slow compared to the CG method. In the combined approach, we use the CG algorithm to rapidly generate a magnetic structure, which is then put into the dynamic solver as an initial estimate. This increases the efficiency of the algorithm by roughly an order of magnitude compared to the dynamic solver alone.

[11] In the CG algorithm, the domain structure is calculated by minimizing the total magnetic energy E_{tot}, which is the sum of the exchange energy ($\propto$ the exchange constant A), the magnetostatic energy ($\propto M_S^2$, where M_S is the spontaneous magnetization), and the anisotropy energy ($\propto$ the first magnetocrystalline anisotropy constant K_1) [*Brown*, 1963]. E_{tot} is calculated using a fast-Fourier transform (FFT) to give a local energy minimum (LEM) for the assemblage. The increased efficiency with which the demagnetizing energy can be calculated in Fourier space allows the high resolution needed to examine large arrays of interacting grains. The dynamic algorithm solves the dynamic Landau-Lifshitz-Gilbert equation. We used a finitely damped solver detailed by *Brown et al*. [1989]. In effect, instead of minimizing the energy, the solver minimizes the torque on each magnetic moment by solving for the effective field.

[12] Values for A (2×10^{-12} Jm^{-1}) and M_S (59 Am^2 $kg^{-1} = 241 \times 10^3$ Am^{-1}) are from *Chang et al*. [2008, 2009]. The value for K_1 ((cubic) (-1.7×10^4 J m^{-3}), which was determined from ferromagnetic resonance (FMR) powder spectra reported by *Winklhofer et al*. (submitted manuscript, 2013), is different to the value reported by *Roberts et al*. [2011] ($+3 \times 10^4$ J m^{-3}). There is still uncertainty about the sign of K_1, because the measured FMR spectra of the greigite powder sample are consistent with two kinds of cubic anisotropy models, one with the $K_1 < 0$ solution used here, the other with $K_1 > 0$ and a large contribution from K_2 ($K_2/K_1 = 3$) (Winklhofer et al., submitted manuscript, 2013). For the lack of an independent physical justification of a large K_2/K_1 ratio in greigite, we here used the $K_1 < 0$ solution, but point out that both anisotropy models are equivalent in terms of the magnetocrystalline anisotropy field (~100 mT).

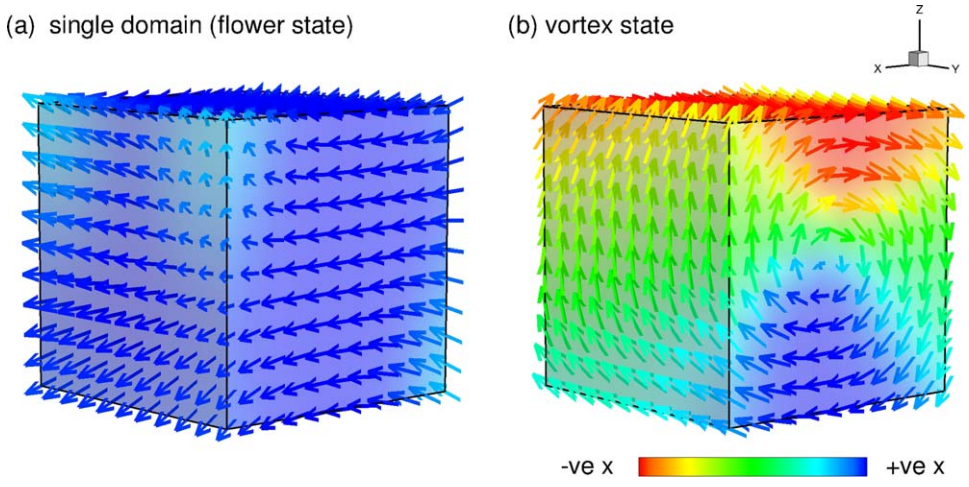

Figure 2. Domain states in cube-shaped grains of greigite at room temperature for a grain with an edge length of 83 nm: (a) single domain (flower state), and (b) single vortex state. In this paper, the term "SD state" refers not just to homogeneous magnetization structures, but also to nonuniform domain structures as shown in (a), which are essentially SD-like with a degree of flowering toward the edges of the grain. In (a) and (b), the crystallographic <100> direction is aligned with the *x* axis.

[13] In determining the SD/MD boundary threshold size (sections 3 and 4 below), the initial CG estimate for the nonuniform magnetic structures in the most elongated grains was found to be effectively the same as the solution produced by the dynamic solver. This convergence between the two algorithms is due to smoothing of the energy surfaces as the grains become more elongated. For more symmetrical grains with more uneven energy surfaces, the CG algorithm can become hooked on small saddle points and trapped in shallow minimum energy states. Therefore, as grains become more elongated, the CG algorithm is less likely to stall and the CG and dynamic solutions converge. Because the CG solver is approximately an order of magnitude faster than the combined algorithm, and it is more memory efficient than the dynamic algorithm for some of the larger arrays, i.e., for the largest chains of elongated grains, calculations were made using only the CG algorithm.

[14] To accurately model nonuniform structures, it is necessary to have a minimum model resolution of two cells per exchange length (exchange length = $\sqrt{(A/K_d)}$, where $K_d = \mu_0 M_S^2/2$ and μ_0 is the permeability of free space [*Rave et al.*, 1998]. For greigite at room temperature the exchange length is 7.5 nm. The minimum resolution was maintained at all times in our calculations, i.e., each cell in the micromagnetic model was ~3.5 nm.

3. SD/MD Critical Sizes for Individual Elongated Grains

[15] There are several methods for determining the SD/MD critical size (d_0). Here the unconstrained method is employed [*Fabian et al.*, 1996; *Witt et al.*, 2005; *Muxworthy and Williams*, 2006]. In this approach, a small grain, say ~20 nm in length, with an initial SD structure (Figure 2a) is gradually increased in size until the domain structure collapses to a vortex (i.e., MD) state at d_{max} (Figures 2b and 3). The grain size is then decreased until the vortex structure becomes SD at d_{min} (Figure 3). The d_{min} and d_{max} values are interpreted to represent the lower and upper bounds, respectively, of a range where both SD and vortex structures can coexist. For the most elongated grains, i.e., AR < 0.4, d_{min} and d_{max} are poorly defined because the collapse is gradual and less abrupt. In such cases, the d_{min} and d_{max} values are estimated at the point where the reduced magnetization passes through 0.8 on the increasing/decreasing curves, where the reduced magnetization is the magnetic moment divided by the magnetic moment of an ideal SD grain.

[16] In addition to calculating d_{min} and d_{max} as a function of AR (Figure 4), we have considered the relationship between the relative orientation of the cubic magnetocrystalline anisotropy [*Roberts*, 1995; *Roberts et al.*, 2011] and the particle elongation for greigite. We model two extreme cases:

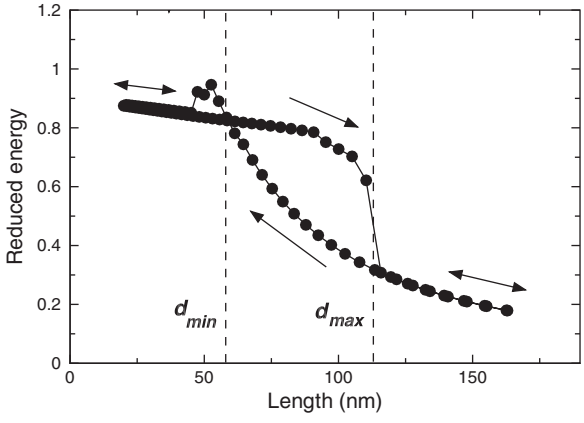

Figure 3. Magnetic energy density of a greigite cube as a function of length for an initial SD configuration (cf. Figure 2a) at room temperature. The grain size was gradually increased until the SD structure collapsed into a vortex structure (cf. Figure 2b) at d_{max} = 107 nm. The size was then gradually decreased until a SD state formed at d_{min} = 58 nm. To maximize computational efficiency, the resolution was increased/decreased with each increase/decrease in size, and the domain structure was rescaled between each pair of calculations. The magnetic energy is normalized by that of a uniform SD structure of the same grain size.

first, where the elongation is in the easy direction (i.e., $\langle 111 \rangle$ axes for $K_1 < 0$) (yielding d_{min}^{easy} and d_{max}^{easy}) and second where it is in the hard direction (d_{min}^{hard} and d_{max}^{hard}). In the scenario with elongation along the easy direction, the magnetocrystalline anisotropy enhances the shape effect, i.e., it encourages the magnetization to align along the elongation axis. In contrast, when the elongation is along the hard direction, the magnetocrystalline anisotropy competes with the shape effect.

[17] In Figure 4, the *y* axis is the particle length, as used by *Butler and Banerjee* [1975] and *Diaz-Ricci and Kirschvink* [1992], rather than the mean diameter as used by *Witt et al*. [2005]. Use of the particle length enables easier comparison with the results of *Diaz-Ricci and Kirschvink* [1992], but the figure is more complicated to understand because the volume of the grains changes with movement along the *x* axis, i.e., there is a change both in shape that contributes to d_0 and in volume that contributes to d_0.

[18] Generally d_{min}^{easy}, d_{max}^{easy}, d_{min}^{hard}, and d_{max}^{hard} increase as AR decreases (Figure 4). The d_{max}^{easy} value is the largest of the four for all values of AR. Orienting the magnetization along the easy axis enhances the effect of elongation, while orientation along the hard direction increases curling of the magnetization at the edges of the grains, which breaks symmetry, encourages nucleation of vortex states and decreases d_0. As AR is reduced, the difference between d_{min}^{easy} and d_{max}^{easy} decreases. The same is true for d_{min}^{hard} and d_{max}^{hard} as the contribution of the magnetocrystalline anisotropy is reduced.

[19] For comparison, the calculated results of *Diaz-Ricci and Kirschvink* [1992] are depicted in Figure 4. Our micromagnetic estimates of the SD/MD threshold size are significantly lower than those obtained from the analytical results of *Diaz-Ricci and Kirschvink* [1992], who lacked experimentally well-constrained material parameters. For example, for a cubic grain, the micromagnetic

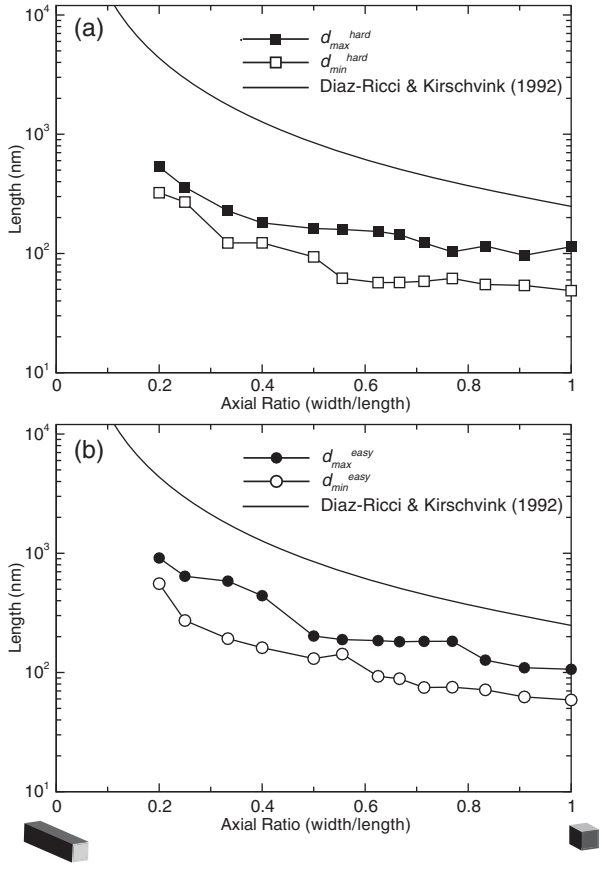

Figure 4. Critical SD to MD threshold lengths (maximum grain dimension) for individual greigite particles as a function of axial ratio (AR). (a) Elongation along the <100> (hard anisotropy for $K_1 < 0$) direction, and (b) along the <111> (easy anisotropy for $K_1 < 0$) direction. Both d_{max} and d_{min} are shown. The lengths were determined using the method defined in Figure 3. For highly elongated grains, i.e., AR < 0.5, d_{max} and d_{min} are poorly defined. For these smaller values of AR, d_{max} and d_{min} were defined as the length where the reduced magnetization passed through 0.8 with increasing/decreasing grain size. AR = 1 is a cube and AR = 0 is an infinitely long rectangular cuboid.

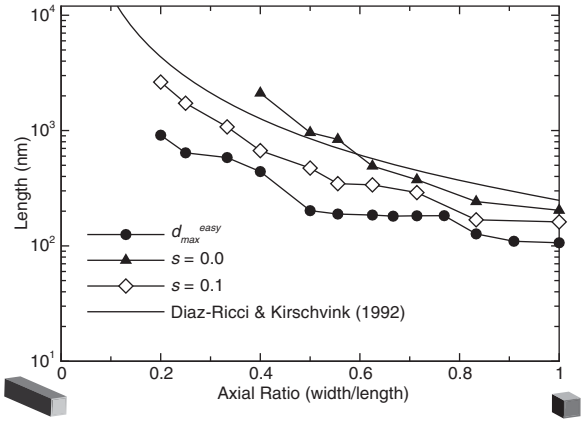

Figure 5. Critical SD to MD threshold lengths (maximum grain dimension) for a chain of interacting greigite grains with varying axial ratios. Grain elongation and chain alignment is in the <111> (easy anisotropy for $K_1 < 0$) direction. The d_0 value was determined from the behavior of the middle grain in a chain of three identical grains with various intergrain spacings s, where s is the interparticle spacing divided by the grain length. Due to insufficient computing memory (maximum 256 GB), calculations of d_0 could not be made for highly interacting elongated particles.

model gives an estimate of ~60 nm (d_{min}) compared to 250 nm from *Diaz-Ricci and Kirschvink* [1992]. This discrepancy can readily be explained by the different parameter combinations used. With $M_S' = 1/2\ M_S$ and $A' = 5\ A$, where the primed and unprimed symbols refer to parameters assumed in *Diaz-Ricci and Kirschvink* [1992] and here, respectively, we obtain for the exchange lengths $L_{ex}' = 4.4\ L_{ex}$. According to the generic d_{min} calculations for equant particles by *Rave et al.* [1998], $d_{min}' = 7.6\ L_{ex}' = 250$ nm for $Q_1' = (K_1/4)/K_d' = 0.027$ and $d_{min} = 7.9\ L_{ex} = 60$ nm for $Q_1 = (-K_1/12)/K_d = 0.12$. Therefore, the threshold SD/MD threshold sizes of *Diaz-Ricci and Kirschvink* [1992] (250 nm) and ours (d_{min} ~60 nm) are in excellent agreement with the respective analytical values d_{min}' and d_{min}.

4. SD/MD Critical Sizes for Magnetostatically Interacting Elongated Grains

[20] To model the effect of magnetostatic interactions on d_0, we consider the behavior of the middle grain in a chain of three grains. Modeling of interactions in this paper was simply done by masking blank cells, setting cell magnetizations to zero, and thereby creating a "void" between neighboring magnetic regions of our finite-difference mesh [*Muxworthy et al.*, 2003b]. We examine the behavior of chains, as opposed to a three-dimensional grid, because this is likely to produce the largest difference compared to noninteracting grains [*Muxworthy and Williams*, 2004], and should be seen as an upper limit: greigite magnetosomes often do not align in linear chains (Figure 1), unlike magnetite magnetosomes. A chain of three grains is short; however, it was chosen so that we could calculate d_0 for elongated grains with large intergrain spacings using a full resolution model (where both the magnetic grains and intergrain spaces contribute to the calculation time). Nevertheless, given the relatively large SD/MD threshold size compared to magnetite, we were unable to calculate the SD/MD threshold size domain phase diagram as completely as *Muxworthy and Williams* [2006] did for magnetite. For example, the largest solutions considered had >10 million elements.

[21] To estimate d_0, a slightly different procedure was used compared to that described above in section 3. Rather than growing the domain structure, an initial SD state was assumed at each grain size, and the model structure was minimized. This procedure produces only a single (upper bound) value for d_0. The only orientation of the magnetocrystalline anisotropy considered was with alignment along the elongation axis, i.e., d_{max}^{easy}. All three grains in the chain had the same magnetocrystalline anisotropy orientation. We considered a number of minimum nontouching separations defined by the ratio s = spacing/length, and calculated d_0 for touching grains, i.e., space/length = 0.0. It is readily seen that both elongation and magnetostatic interactions cause significantly increased d_0 (Figure 5). For cubic grains, the increase is from (d_{max} =) 107 to (d_0 =) 204 nm (Figure 5).

5. SP/SD Critical Sizes for Individual and Magnetostatically Interacting Elongated Grains

[22] SD grains below a certain critical volume (the blocking volume, v_b) are magnetically unstable and have SP behavior. In systems of interacting SD grains, both SP and stable SD grains contribute to the interaction field. The magnetic interaction field generated by a stable SD grain is constant during rotation of a neighboring interacting SP or stable SD grain. This makes it possible to treat magnetic interaction fields due to stable SD grains as effectively static [*Spinu and Stancu*, 1998]. The effect of magnetostatic interactions due to stable

SD grains is to increase/decrease the (micro)coercive (H_K) force of a crystal by the interaction field $\pm H_S$ [*Dunlop and West*, 1969]. For SP grains, the situation is more complicated. The behavior of a magnetic assemblage of SP particles falls into one of three regimes depending on the interparticle interactions [*Dormann et al*., 1997]: (i) a pure SP case (noninteracting), (ii) an SP state modified by interactions, and (iii) a collective state.

[23] The properties of state (iii), which is called the glass collective state [*Dormann et al*., 1999], are close to those of spin glasses with a phase transition. This state is not fully understood and there is no analytical model for the collective state. However, *Muxworthy and Williams* [2009] showed that for chains of nearly identical, interacting grains, it is only necessary to consider state (ii), an SP state modified by magnetostatic interactions. The interaction field due to SP grains fluctuates at a high rate near the blocking volume or blocking temperature where relaxation is important. These dynamic interactions are qualitatively different from static ones. Dynamic systems are not in thermodynamic equilibrium and hence cannot be directly modeled using Boltzmann statistics. Several approaches have been developed to address this problem [*Dormann et al*., 1988]. These models demonstrate that the effect of interactions due to SP grains is to increase the relaxation time t_m, given by *Néel* [1949]:

$$t_m = \tau_0 \exp(E_B/kT) \tag{1}$$

by increasing the energy barrier $E_B = E_A$ (where E_A is the anisotropy energy barrier), by an amount termed the interaction energy E_{int}, i.e., $E_B = E_A + E_{int}$, where k is Boltzmann's constant, T is the temperature and τ_0 is the atomic reorganization time ($\sim 10^{-9}$) [*Worm*, 1998]. The relaxation time t_m can be a few nanoseconds for SP particles that undergo thermal relaxation during laboratory experiments to billions of years for stable SD particles in geological samples.

[24] For an SD assemblage with both dynamic SP and static stable SD interactions, using the experimentally verified theory of *Dormann et al*. [1988] and *Muxworthy* [2001] showed that the blocking volume, v_b, is given by:

$$v_b = \frac{-E_{\text{int}} + 2kT(\ln(t_m/\tau_0)}{\mu_0 M_S (H_K \pm H_S)} \tag{2}$$

where μ_0 is the permeability of free space. This equation is strictly for a system with only two possible states; however, in elongated and highly interacting chains this is likely to be the case. For symmetrical samples with higher order magnetocrystalline anisotropy, small errors will occur in blocking volume estimations.

5.1. Determining the Blocking Volume for a Chain of Identical Grains: A Model for Magnetosome Crystals

[25] For SD assemblages with identically shaped particles and a distribution of grain volumes, it is necessary to calculate both E_{int} and H_S [*Muxworthy*, 2001]. However, *Muxworthy and Williams* [2009] argued that if it is assumed that every grain is either blocked or unblocked, i.e., all particles including the end grains have identical behavior, then the blocking volume is the volume where the magnetostatic interaction fields alone, i.e., $E_{int} \equiv 0$, are sufficient to overcome the thermal fluctuation fields. All that is required to find the blocking volume of a chain of identical grains is the value of H_S such that $H_K \pm H_S$ ($\equiv$ the coercive force H_C) overcomes thermal fluctuations.

[26] *Muxworthy and Williams* [2009] determined H_C using a micromagnetic hysteresis simulation and demonstrated that a chain of only seven particles was sufficient. They argued that only hysteresis needs to be calculated for a simulated field applied along the chain length if the grain elongation and chain-length extension are aligned. Nevertheless, this approach provides only a lower limit for the SP/SD threshold for particles with nonuniaxial anisotropy: the application of an external field distorts the energy surface, therefore the in-field energy barrier determined using this approach will not have the same structure as the zero-field barrier. The relative degree of distortion will decrease as the interaction field increases, i.e., this assumption is more appropriate for strongly interacting magnetic particles.

[27] In this study, we determine the SP/SD threshold for single crystals and chains of interacting greigite grains, where the grain elongation and chain alignment is along the easy axis (here one of the <111> axes of the cubic system). For single crystals, we directly determined the energy barrier (equation (1)) from the anisotropy energy surface, i.e., a combination of the uniaxial shape anisotropy and the cubic magnetocrystalline anisotropy. For the interacting chains, the blocking volume was determined using equation (2) by first numerically calculating H_C for a range of axial ratios. We only consider the case where the grains are touching

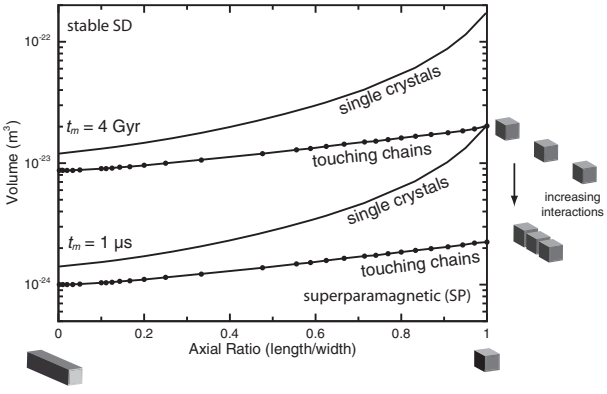

Figure 6. Blocking volume curves on a volume versus axial ratio for single crystals and touching chains of greigite. Grain elongation and chain alignment is in the <111> direction. Two relaxation times t_m are shown: 1 μs and 4 Gyr. The blocking volumes were determined directly from equation (1) for the single crystals, and for the touching grains by numerically solving equation (2).

because this is the most reliable solution and represents the extreme limiting case. The model includes both the cubic magnetocrystalline anisotropy of greigite plus a "shape anisotropy," which is calculated in the magnetostatic energy term. Values of $t_m = 1$ μs and 4 Gyr are plotted against grain volume in Figure 6. For single crystals, v_b decreases with increasing elongation (decreasing AR), in agreement with calculations for magnetite [*Butler and Banerjee*, 1975; *Winklhofer et al*., 1997; *Muxworthy and Williams*, 2009; *Newell*, 2009] and greigite [*Diaz-Ricci and Kirschvink*, 1992].

[28] In the interacting models, H_S (equation (2)) was positive. Generally, for systems with two and three-dimensional magnetostatic interaction fields, H_S is negative [*Muxworthy and Williams*, 2004]. Here it is positive because the particles are in a chain, which produces a linear interaction field. Positive magnetostatic interactions effectively increase H_C, which results in a reduction of v_b (Figure 6), i.e., interactions decrease the SP to stable SD transition boundary. As the degree of interaction increases, v_b decreases.

[29] The blocking volume was determined for interacting chains for $t_m = 1$ μs and 4 Gyr (Figure 6). As was shown by *Néel* [1949] for individual grains, increasing the relaxation time results in increased blocking volume. The longer timescale was chosen because of potential interests in magnetic stabilities over the age of the Earth, while the shortest timescale is an extreme case to demonstrate variability in t_m.

6. Domain-State Phase Diagram

[30] We have constructed a domain-state phase diagram for interacting chains of elongated greigite particles (Figure 7). Interactions both decrease the SP to stable SD transition size for chains of SD grains and increase the SD to MD transition size, which significantly expands the SD size range. For the SP/SD transition, an intermediate timescale of $t_m = 100{,}000$ s represents the stability time required for magnetotaxis (same order of magnitude as the lifespan of a bacteria). For example, for AR = 1 and $t_m = 100{,}000$ s, the noninteracting SD range is 46 nm < length < 107 nm, which increases to 23 nm < length < 204 nm for chains of touching grains. Although the absolute values for the critical domain-state threshold sizes are different to those for magnetite, the trends are the same. For comparison, interactions increase the SD to MD threshold size in a chain of magnetite from 73 nm for noninteracting grains to 198 nm for touching grains [*Muxworthy and Williams*, 2006]. The reason for the difference in absolute

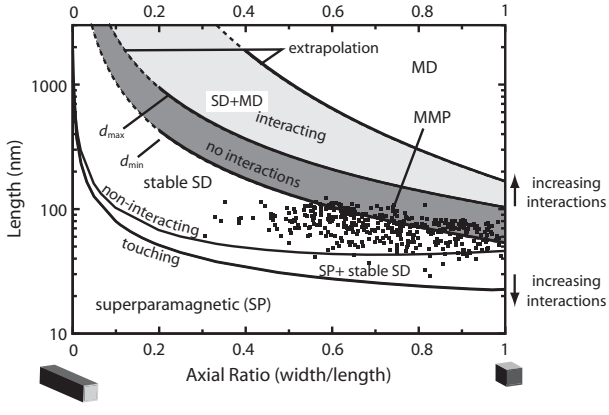

Figure 7. Stable SD grain size ranges for individual particles and for chains of interacting greigite magnetosomes. Grain elongation and chain alignment is in the <111> direction. Published observational data for MMP greigite magnetosomes [*Pósfai et al*., 2001] are plotted. Using the format of *Butler and Banerjee* [1975], length (long-axis) rather than volume is plotted versus AR for various grain spacing/length ratios. Use of length enables easier comparison with *Butler and Banerjee* [1975], but the figure is more complicated to understand because the particle volume changes across the *x* axis, i.e., there is a change in both shape and volume that contributes to the critical boundaries. Hence, the blocking size appears to increase with particle elongation, unlike in Figure 6. For noninteracting particles, there is a range of grain sizes marked by d_{min} and d_{max} where both SD and MD states are possible. For the SP/SD transition an intermediate timescale of $t_m = 100{,}000$ s represents the stability time required for magnetotaxis.

size for the domain-state thresholds is due to relative differences in values for the exchange energy, spontaneous magnetization and magnetocrystalline anisotropy for the two minerals.

6.1. Model Uncertainties

[31] There are empirical errors associated with the three input constants used in the model: M_S, A, and K_1. The error in M_S is thought to be relatively small and insignificant, but the uncertainty in the other two parameters is likely to be greater and potentially important.

[32] An accurate determination of A requires inelastic neutron scattering experiments to be carried out on a large single crystal of greigite. Due to the difficulty in producing large stoichiometric samples of greigite, *Chang et al*. [2008] estimated A by studying powdered samples and fitting a Bloch law to an M_S versus temperature curve; hence, the estimate for A should be considered a good estimate rather than a definitive answer. *Rave et al*. [1998] showed the critical SD/MD threshold size scales with the exchange length $\propto \sqrt{A}$, i.e., a twofold increase in A would increase d_{max} by about 40%. The error in A was not quantified by *Chang et al*. [2008], but could be as high as 50–80%. The K_1 used in this study has recently been determined using ferromagnetic resonance spectroscopy (FMR) on a greigite powder sample (Winklhofer et al., submitted manuscript, 2013). Ideally K_1 should be determined from single-crystal measurements (torque curves, FMR spectra) on a large oriented crystal, therefore; again, the estimate for K_1 is subject to an error. However, unlike the error in the exchange constant, the response of a magnetic domain structure to variation in K_1 is nonlinear making it difficult to quantify the effect this error will have on the SD/MD threshold size. Results from initial calculations based on an earlier estimate of K_1 ($+3 \times 10^4$ J m^{-3}, $Q_1 = 0.2$) are shown in the supporting information[1] (Figures S1–S3). The change in sign of K_1 changes the easy direction to the <100> direction. It can be seen that a larger $|K_1|$ significantly increases the upper SD/MD limit size d_{max}, i.e., it stabilizes the metastable SD state, particularly when the elongation is along the easy crystal axis. The effect on the lower SD/MD limit size d_{min} is not so pronounced; e.g., for equant particles, d_{min} changes from 60 to 70 nm when going from $Q_1 = 0.04$ to $Q_1 = 0.2$. Since the SP limit size decreases with increasing $|K_1|$, the combined effect of a larger $|K_1|$ is an enlargement of both the stable and metastable SD field in the phase diagram.

6.2. Comparison with Greigite Magnetosome Data

[33] Plotted in Figure 7 are observational data from *Pósfai et al*. [2001] for MMP greigite magnetosomes. Most of these magnetosome sizes plot well below the noninteracting SD/MD threshold size, which suggests that they have magnetically stable SD sizes regardless of the degree of magnetostatic interactions; MMP magnetosomes are usually found in poorly defined chains, i.e., they are weakly interacting [*Pósfai et al*., 1998, 2001; *Kasama et al*., 2006a, 2006b; *Winklhofer et al*., 2007]. *Winklhofer et al*. [2007] showed experimentally that interactions in MMP greigite stabilize the remanence state of clustered SP and SD particles.

[34] *Pósfai et al*. [2001] also reported that greigite particles from a Miocene marl from Poland (´aöka) have grain size and AR distribution shapes that are similar to those for MMP bacteria. *Pósfai et al*. [2001] hypothesized that these greigite particles are magnetofossils, with the largest crystals being 240 nm in size (AR ~0.7), i.e., above the noninteracting SD/MD threshold size, but within the size range for stable SD behavior for magnetically interacting particles (Figure 7). Other observations of suggested greigite magnetofossils [e.g., *Vasiliev et al*., 2008] also fall within the stable SD range.

7. Conclusions

[35] Using a three-dimensional micromagnetic algorithm, we have calculated and constructed the first domain-state phase diagram for interacting chains of elongated greigite particles (Figure 7). As was found for magnetite [*Muxworthy and Williams*, 2006, 2009], interactions both decrease the SP to stable SD transition size for chains of SD grains and they increase the SD to MD transition size, which significantly expands the SD size range. For cubic greigite grains, the SD range for noninteracting SD grains is increased from 46 nm < length < 107 nm (t_m = 100,000 s) to 23 nm < length < 204 nm for chains of touching grains.

[36] Most published greigite magnetosome sizes plot well below the noninteracting SD/MD threshold size (Figure 7). Although greigite has a smaller spontaneous magnetization than magnetite

(~64%) [*Chang et al.*, 2008], the larger SD/MD threshold size means that, regardless of interactions, it is possible for SD greigite particles to produce magnetic signals that are more than twice as large as those for magnetite particles.

Acknowledgment

[37] This work was funded by NERC grant NE/G004617/1.

References

Bazylinski, D. A., R. B. Frankel, B. R. Heywood, S. Mann, J. W. King, P. L. Donaghay, and A. K. Hanson (1995), Controlled biomineralization of magnetite (Fe_3O_4) and greigite (Fe_3S_4) in a magnetotactic bacterium, *Appl. Environ. Microbiol.*, *61*, 3232–3239.

Brown, W. F., Jr.(1963), Micromagnetics, John Wiley, New York.

Brown, P. N., G. D. Byrne, and A. C. Hindmarsh (1989), VODE: A variable coefficient ODE solver, *SIAM J. Sci. Stat. Comput.*, *10*, 1038–1051.

Butler, R. F., and S. K. Banerjee (1975), Theoretical single-domain grain size range in magnetite and titanomagnetite, *J. Geophys. Res.*, *80*, 4049–4058, doi:10.1029/JB080i029p04049.

Chang, L., A. P. Roberts, Y. Tang, B. D. Rainford, A. R. Muxworthy, and Q. W. Chen (2008), Fundamental magnetic parameters from pure synthetic greigite (Fe_3S_4), *J. Geophys. Res.*, *113*, B06104, doi:10.1029/2007JB005502.

Chang, L., B. D. Rainford, J. R. Stewart, C. Ritter, A. P. Roberts, Y. Tang, and Q. W. Chen (2009), Magnetic structure of greigite (Fe_3S_4) probed by neutron powder diffraction and polarized neutron diffraction, *J. Geophys. Res.*, *114*, B07101, doi:10.1029/2008JB006260.

Chang, L., A. P. Roberts, W. Williams, J. D. Fitz Gerald, J. C. Larrasoaña, L. Jovane, and A. R. Muxworthy (2012), Giant magnetofossils and hyperthermal events, *Earth Planet. Sci. Lett.*, *351–352*, 258–269, doi:10.1016/j.epsl.2012.07.031.

Diaz-Ricci, J. C. D., and J. L. Kirschvink (1992), Magnetic domain state and coercivity predictions for biogenic greigite (Fe_3S_4)—A comparison of theory with magnetosome observations, *J. Geophys. Res.*, *97*, 17,309–17,315.

Dormann, J. L., L. Bessais, and D. Fiorani (1988), A dynamic study of small interacting particles—Superparamagnetic model and spin-glass laws, *J. Phys. C Solid State Phys.*, *21*, 2015–2034, doi:10.1088/0022–3719/21/10/019.

Dormann, J. L., D. Fiorani, and E. Tronc (1997), Magnetic relaxation in fine-particle systems, *Adv. Chem. Phys.*, *98*, 283–494, doi:10.1002/9780470141571.ch4.

Dormann, J. L., D. Fiorani, and E. Tronc (1999), On the models for interparticle interactions in nanoparticle assemblies: Comparison with experimental results, *J. Magn. Magn. Mater.*, *202*, 251–267, doi:10.1016/S0304-8853(98)00627-1.

Dunin-Borkowski, R. E., M. R. McCartney, R. B. Frankel, D. A. Bazylinski, M. Pósfai, and P. R. Buseck (1998), Magnetic microstructure of magnetotactic bacteria by electron holography, *Science*, *282*, 1868–1870, doi:10.1126/science.282.5395.1868.

Dunlop, D. J., and G. F. West (1969), An experimental evaluation of single-domain theories, *Rev. Geophys.*, *7*, 709–757.

Evans, M. E., and M. W. McElhinny (1969), The origin of stable remanence in magnetite-bearing igneous rocks, *J. Geomagn. Geoelectr.*, *21*, 757–773.

Fabian, K., A. Kirchner, W. Williams, F. Heider, T. Leibl, and A. Huber (1996), Three-dimensional micromagnetic calculations for magnetite using FFT, *Geophys. J. Int.*, *124*, 89–104, doi:10.1111/j.1365-246X.1996.tb06354.x.

Faivre, D., and D. Schüler (2008), Magnetotactic bacteria and magnetosomes, *Chem. Rev.*, *108*, 4875–4898, doi:10.1021/CR078258W.

Frankel, R. B., J. P. Zhang, and D. A. Bazylinski (1998), Single magnetic domains in magnetotactic bacteria, *J. Geophys. Res.*, *103*, 30,601–30,604, doi:10.1029/97JB03512.

Kasama, T., M. Pósfai, R. K. K. Chong, A. P. Finlayson, R. E. Dunin-Borkowski, and R. B. Frankel (2006a), Magnetic microstructure of iron sulfide crystals in magnetotactic bacteria from off-axis electron holography, *Physica B*, *384*, 249–252, doi:10.1016/j.physb.2006.06.002.

Kasama, T., M. Pósfai, R. K. K. Chong, A. P. Finlayson, P. R. Buseck, R. B. Frankel, and R. E. Dunin-Borkowski (2006b), Magnetic properties, microstructure, composition, and morphology of greigite nanocrystals in magnetotactic bacteria from electron holography and tomography, *Am. Mineral.*, *91*, 1216–1229, doi:10.2138/am.2006.2227.

Kopp, R. E., and J. L. Kirschvink (2008), The identification and biogeochemical interpretation of fossil magnetotactic bacteria, *Earth Sci. Rev.*, *86*, 42–61, doi:10.1016/J.EARSCIREV.2007.08.001.

Lins, U., M. R. McCartney, M. Farina, R. B. Frankel, and P. R. Buseck (2005), Habits of magnetosome crystals in coccoid magnetotactic bacteria, *Appl. Environ. Microbiol.*, *71*, 4902–4905, doi:10.1128/AEM.71.8.4902–4905.2005.

Lowenstam, H. A. (1962), Magnetite in denticle capping in recent chitons (Polyplacophora), *Geol. Soc. Am. Bull.*, *73*, 435–438.

McCartney, M. R., U. Lins, M. Farina, P. R. Buseck, and R. B. Frankel (2001), Magnetic microstructure of bacterial magnetite by electron holography, *Eur. J. Mineral.*, *13*, 685–689.

Muxworthy, A. R. (2001), Effect of grain interactions on the frequency dependence of magnetic susceptibility, *Geophys. J. Int.*, *144*, 441–447, doi:10.1046/j.1365-246x.2001.00342.x.

Muxworthy, A. R., and W. Williams (2004), Distribution anisotropy: The influence of magnetic interactions on the anisotropy of magnetic remanence, in *Magnetic Fabric: Methods and Applications*, edited by F. Martín-Hernández et al., Geological Society, London, Special Publications, pp. 37–47.

Muxworthy, A. R., and W. Williams (2006), Critical single-domain/multidomain grain-sizes in non-interacting and interacting elongated magnetite particles: Implications for magnetosomes, *J. Geophys. Res.*, *111*, B12S12, doi:10.1029/2006JB004588.

Muxworthy, A. R., and W. Williams (2009), Critical superparamagnetic/single-domain grain sizes in interacting magnetite particles: Implications for magnetosome crystals, *J. R. Soc. Interf.*, *6*, 1207–1212, doi:10.1098/RSIF.2008.0462.

Muxworthy, A. R., D. J. Dunlop, and W. Williams (2003a), High-temperature magnetic stability of small magnetite particles, *J. Geophys. Res.*, *108*(B5), 2281, doi:10.1029/2002JB002195.

Muxworthy, A. R., W. Williams, and D. Virdee (2003b), Effect of magnetostatic interactions on the hysteresis parameters of single-domain and pseudo-single-domain grains, *J. Geophys. Res.*, *108*(B11), 2517, doi:10.1029/2003JB002588.

Néel, L. (1949), Théorie du traînage magnétique des ferromagnétiques en grains fins avec applications aux terres cuites, *Ann. Geophys.*, *5*, 99–136.

Newell, A. J. (2009), Transition to superparamagnetism in chains of magnetosome crystals, *Geochem. Geophys. Geosyst.*, *10*, Q11Z08, doi:10.1029/2009GC002538.

Newell, A. J., and R. T. Merrill (1999), Single-domain critical sizes for coercivity and remanence, *J. Geophys. Res.*, *104*, 617–628, doi:10.1029/1998JB900039.

Perantoni, M., D. M. S. Esquivel, E. Wajnberg, D. Acosta-Avalos, G. Cernicchiaro, and H. L. de Barros (2009), Magnetic properties of the microorganism *Candidatus Magnetoglobus multicellularis*, *Naturwissenschaften*, *96*, 685–690, doi:10.1007/s00114-009-0520-2.

Pósfai, M., P. R. Buseck, D. A. Bazylinski, and R. B. Frankel (1998), Iron sulfides from magnetotactic bacteria: Structure, composition, and phase transitions, *Am. Mineral.*, *83*, 1469–1481.

Pósfai, M., K. Cziner, E. Márton, P. Márton, P. R. Buseck, R. B. Frankel, and D. A. Bazylinski (2001), Crystal-size distributions and possible biogenic origin of Fe sulfides, *Eur. J. Mineral.*, *13*, 691–703, doi:10.1127/0935-1221/2001/0013-0691.

Rave, W., K. Fabian, and A. Hubert (1998), The magnetic states of small cubic magnetic particles with uniaxial anisotropy, *J. Magn. Magn. Mater.*, *190*, 332–348, doi:10.1016/S0304–8853(98)00328-X.

Roberts, A. P. (1995), Magnetic properties of sedimentary greigite (Fe_3S_4), *Earth Planet. Sci. Lett.*, *134*, 227–236.

Roberts, A. P., L. Chang, C. J. Rowan, C. S. Horng, and F. Florindo (2011), Magnetic properties of sedimentary greigite (Fe_3S_4): An update, *Rev. Geophys.*, *49*, RG1002, doi:10.1029/2010RG000336.

Rowan, C. J., and A. P. Roberts (2006), Magnetite dissolution, diachronous greigite formation, and secondary magnetizations from pyrite oxidation: Unravelling complex magnetizations in Neogene marine sediments from New Zealand, *Earth Planet. Sci. Lett.*, *241*, 119–137, doi:10.1016/j.epsl.2005.10.017.

Schumann, D., et al. (2008), Gigantism in unique biogenic magnetite at the Paleocene-Eocene Thermal Maximum, *Proc. Natl. Acad. Sci. U.S.A.*, *105*, 17,648–17,653, doi:10.1073/pnas.0803634105.

Silveira, T. S., J. L. Martins, K. T. Silva, F. Abreu, and U. Lins (2007), Microscopy studies on uncultivated magnetotactic bacteria, in Modern Research and Educational Topics in Microscopy, edited by A. Méndez-Vilas and J. Díaz, pp. 111–121, Formatex, Badajoz, Spain.

Spinu, L., and A. Stancu (1998), Modelling magnetic relaxation phenomena in fine particles systems with a Preisach-Néel model, *J. Magn. Magn. Mater.*, *189*, 106–114, doi:10.1016/S0304–8853(98)00205-4.

Suess, D., V. Tsiantos, T. Schrefl, J. Fidler, W. Scholz, H. Forster, R. Dittrich, and J. J. Miles (2002), Time resolved micromagnetics using a preconditioned time integration method, *J. Magn. Magn. Mater.*, *248*, 298–311, doi:10.1016/S0304-8853(02)00341-4.

Suzuki, Y., et al. (2006), Sclerite formation in the hydrothermal-vent "scaly-foot" gastropod—Possible control of iron sulfide biomineralization by the animal, *Earth Planet. Sci. Lett.*, *242*, 39–50, doi:10.1016/j.epsl.2005.11.029.

Thomas-Keprta, K. L., D. A. Bazylinski, J. L. Kirschvink, S. J. Clemett, D. S. McKay, S. J. Wentworth, H. Vali, E. K. Gibson Jr., and C. S. Romanek (2000), Elongated prismatic magnetite crystals in ALH 84001 carbonate globules: Potential Martian magnetofossils, *Geochim. Cosmochim. Acta*, *64*, 4049–4081, doi:10.1016/S0016-7037(00)00481-6.

Vasiliev, I., C. Franke, J. D. Meeldijk, M. J. Dekkers, C. G. Langereis, and W. Krijgsman (2008), Putative greigite magnetofossils from the Pliocene epoch, *Nat. Geosci.*, *1*, 782–786, doi:10.1038/ngeo335.

Warén, A., S. Bengtson, S. K. Goffredi, and C. L. Van Dover (2003), A hot-vent gastropod with iron sulfide dermal sclerites, *Science*, *302*, 1007, doi:10.1126/science.1087696.

Williams, W., and D. J. Dunlop (1989), Three-dimensional micromagnetic modelling of ferromagnetic domain structure, *Nature*, *337*, 634–637, doi:10.1038/337634a0.

Winklhofer, M., K. Fabian, and F. Heider (1997), Magnetic blocking temperatures of magnetite calculated with a three-dimensional micromagnetic model, *J. Geophys. Res.*, *102*, 22,695–22,709, doi:10.1029/97JB01730.

Winklhofer, M., L. G. Abraxcado, A. F. Davila, C. N. Keim, and H. G. P. Lins de Barros (2007), Magnetic optimization in a Multicellular Magnetotactic Organism, *Biophys. J.*, *82*, 661–670.

Witt, A., K. Fabian, and U. Bleil (2005), Three-dimensional micromagnetic calculations for naturally shaped magnetite: Octahedra and magnetosomes, *Earth Planet. Sci. Lett.*, *233*, 311–324, doi:10.1016/j.epsl.2005.01.043.

Worm, H.-U. (1998), On the superparamagnetic-stable single domain transition for magnetite, and frequency dependence of susceptibility, *Geophys. J. Int.*, *133*, 201–206, doi:10.1046/j.1365-246X.1998.1331468.x.